Published in final edited form as:
Mol Pharm. 2009 ; 6(6): 1891–1902. doi:10.1021/mp900215p.

Impact of hydrogel nanoparticle size and functionalization on in vivo behavior for lung imaging and therapeutics

Yongjian Liu[1,4], **Aida Ibricevic-Richardson**[2,4], **Joel A. Cohen**[3,4], **Jessica L. Cohen**[3], **Sean P. Gunsten**[2], **Jean M. J. Fréchet**[3], **Michael J. Walter**[2], **Michael J. Welch**[1], and **Steven L. Brody**[2,*]

[1]Department of Radiology, Washington University School of Medicine, St. Louis, MO 63110

[2]Department of Internal Medicine, Washington University School of Medicine, St. Louis, MO 63110

[3]College of Chemistry, University of California, Berkeley, CA, 94720

Abstract

Polymer chemistry offers the possibility of synthesizing multifunctional nanoparticles which incorporate moieties that enhance diagnostic and therapeutic targeting of cargo delivery to the lung. However, since rules for predicting particle behavior following modification are not well defined, it is essential that probes for tracking fate in vivo are also included. Accordingly, we designed polyacrylamide-based hydrogel particles of differing sizes, functionalized with a nona-arginine cell-penetrating peptide (Arg_9), and labeled with imaging components to assess lung retention and cellular uptake after intratracheal administration. Radiolabeled microparticles (1–5 μm diameter) and nanoparticles (20–40 nm diameter) without and with Arg_9 showed diffuse airspace distribution by positron emission tomography imaging. Biodistribution studies revealed that particle clearance and extrapulmonary distribution was, in part, size dependent. Microparticles were rapidly cleared by mucociliary routes but unexpectedly, also through the circulation. In contrast, nanoparticles had prolonged lung retention enhanced by Arg_9 and were significantly restricted to the lung. For all particle types, uptake was predominant in alveolar macrophages, and, to a lesser extent, lung epithelial cells. In general, particles did not induce local inflammatory responses, with the exception of microparticles bearing Arg_9. Whereas microparticles may be advantageous for short-term applications, nano-sized particles constitute an efficient high-retention and non-inflammatory vehicle for the delivery of diagnostic imaging agents and therapeutics to lung airspaces and alveolar macrophages that can be enhanced by Arg_9. Importantly, our results show that minor particle modifications may significantly impact in vivo behavior within the complex environments of the lung, underscoring the need for animal modeling.

Keywords

cell penetrating peptide; lung; macrophage; mice; microparticle; nanoparticle; polyacrylamide; polyarginine; positron emission tomography

*Address correspondence to: Steven L. Brody, Washington University School of Medicine, Box 8052, 660 South Euclid Avenue, St. Louis, MO 63110, USA; Phone: (314) 362-8969; Fax (314) 362-8987, brodys@wustl.edu.

[4]These authors contributed equally to this work.

SUPPORTING INFORMATION AVAILABLE: Synthesis of N-acryloyltyramine. This information is available free of charge via the Internet at http://pubs.acs.org/.

INTRODUCTION

Polymer chemistry offers the capacity to generate a wide variety of nanoparticles with diverse classes of functional groups to provide unique possibilities for diagnostic imaging and therapy.[1–3] Tailoring particles with specialized functions can therefore enhance behavior in specific organs or cell microenvironments.[4, 5] In this regard, each disease target presents challenges related to the route of administration, the properties of the particle system, and the biologic responses. Acute and chronic respiratory diseases caused by infectious, inflammatory and genetic etiologies have a high morbidity and mortality and are thus excellent candidates for novel nanotechnology-based diagnostic and treatment strategies.[6–8] The respiratory tract provides an easily accessed route for organ-specific delivery, with an established record of success for inhaled drug therapies and nuclear imaging. To date, the primary focus of evaluation of nanoparticles in the respiratory tract has been on the toxicity of environmental particulate pollutants and metal particles.[9, 10] Thus, the development of synthetic nanoparticles for delivery to the respiratory tract for clinical application is still in its early stages, and the effects of structural features, components for imaging, cell targeting and permeation on in vivo particle behavior are not yet well defined.[6–8]

Existing polymeric particle systems for lung delivery are primarily composed of hydrophobic materials such as poly(lactic-*co*-glycolic acid) (PLGA) chains condensed into particles and dispersion-polymerized poly(butyl cyanoacrylate) particles.8, 11 Few systems for lung delivery have been explored that employ hydrophilic polymer platforms based on crosslinked hydrogels. Our group has recently described the synthesis of hydrogel-based polyacrylamide microparticles (PMP, 1–5 μm diameter) and nanoparticles (PNP, <100 nm diameter) that can be tuned for size and degradation rate through the incorporation of pH-sensitive crosslinks, and functionalized to carry cargoes such as imaging probes, proteins, or nucleic acids.12–16 In addition, small molecules and peptides for targeting and improved cell uptake can be built into the particle backbone through copolymerization. These modifications are especially important in the case of non-malignant lung diseases where the phenomenon of Enhanced Permeability and Retention (EPR) and tumor-specific cell membrane targets are not applicable.17 Thus, we have been particularly interested in functionalizing PMP and PNP with cell-penetrating peptides (CPPs) that may increase cellular uptake of particles in vivo and display mucoadhesive characteristics in the lung.18

CPPs are short cationic peptides derived from biological sources, including the HIV TAT (trans-activator of transcription) protein.[19] Over the past 20 years, numerous studies have demonstrated that naturally occurring or synthetic CPPs such as oligomers of arginine (e.g., the nona-arginine; Arg_9) enhance the cellular uptake of proteins, nucleic acids, drugs, and nanoparticles.[20–22] Similarly, we have demonstrated that modifying PMP with Arg_9 enhances cellular particle uptake in vitro.[12] However, only a few reports have described CPP-mediated transport of molecules in the lung. In pioneering studies, intraperitoneal or intravenous injection of a TAT-bound protein was shown to result in uptake in multiple organs including low quantities in the lungs, although the cell type targeted was not identified.[23, 24] More recently, TAT bound to plasmid DNA encoding a luciferase reporter administered intratracheally to mice was found to be superior to plasmid alone for enhancing transfection efficiency, albeit with low levels of luciferase expression and accompanied by lung inflammation.[25] In contrast, gene silencing with siRNA conjugated to TAT delivered intratracheally was not superior to siRNA alone.[26] Thus, while potentially powerful, the value of CPP-modified structures is not well understood for lung delivery. Moreover, there is little information available to guide the design and assessment of particulate carrier systems complexed with CPPs for respiratory tract delivery.

In this work, we hypothesized that both particle size and functionalization with Arg_9 would significantly impact particle behavior in the lung as characterized by retention, cell uptake and immune response. We thus focused on interactions of particles of varying sizes and surface modification with the airspace environment, epithelial and immune cells, and extra-pulmonary organs. Additionally, since it has been shown that particles can rapidly move out of the lung to other organs, we used imaging and biodistribution studies as critical assays for understanding particle fate in vivo.[27] We took advantage of our ability to incorporate multiple imaging probes to enable (i) non-invasive tracking of particles in vivo using positron emission tomography, (ii) quantification of specific organ distribution, and (iii) analysis of cellular uptake following intratracheal delivery. Finally, with concern for minimizing particle-associated inflammatory responses, we assessed the presence of markers of lung inflammation following instillation of PMP and PNP into the lungs.

EXPERIMENTAL PROCEDURES

General Procedures and Materials for Particle Synthesis

Unless otherwise noted, all chemicals were purchased from Sigma-Aldrich and used without additional purification. Acrylamide, *N*,*N*'-methylene-bis-acrylamide, ammonium persulfate, and *N*,*N*,*N*',*N*'-tetramethylethylene-diamine (TMEDA) were purchased from Bio-Rad. The cell-penetrating peptide (CPP) consisting of nine arginine residues (Arg_9, acrylamide-R_9-COOH) was purchased from Applied Peptech Suzhou. Hexane (OmniSolv grade) was purchased from EMD. UltraPure 0.1-μm filtered water, and phosphate buffered saline (PBS, pH 7.4) were purchased from Invitrogen.

Synthesis of Polyacrylamide Nanoparticles (PNP)

PNP encapsulating bovine serum albumin conjugated with Alexa Fluor 488 (BSA-488, Invitrogen) and either modified or not modified with Arg_9 (Figure 1) were prepared using modifications to a previously reported method.[13] Briefly, AOT (237 mg, 0.53 mmol) and Brij 30 (459 mg, 1.27 mmol) were added to a 20 mL glass vial. The vial was sealed with a Teflon-lined septum cap and purged with dry nitrogen for 10 min. All further solutions were added to the vial *via* syringe. Deoxygenated hexane (10 mL) was added to the vial and vortexed to completely dissolve the surfactants. Separately, BSA-488 (0.57 mg) was dissolved in PBS (pH 9, 285 μL), to which acrylamide (61.3 mg, 862 μmol), N,N'-methylene-bis-acrylamide (7.10 mg, 46.0 μmol), N-acryloyltyramine (1.80 mg, 9.41 μmol, see Supporting Information for synthesis), and Arg_9 (1.30 mg, 0.88 μmol) were added and dissolved. Dry nitrogen was bubbled through the monomer solution for 2 min, and then 255 μL of this solution was added to the surfactant solution. The vial was vortexed to form a stable microemulsion. A 50% (w/v) solution of ammonium persulfate in PBS (pH 9, 16 μL) was then added to the emulsion while vortexing. After 5 min, polymerization was initiated by the addition of TMEDA (25 μL), and the mixture was vortexed at 600 rpm at room temperature for 30 min. The solvent was evaporated, and absolute ethanol (10 mL) was added, resulting in a milky-white suspension. The particles were isolated by centrifugation (2000 × *g*, room temperature, 5 min), and washed with absolute ethanol (5 × 10 mL), centrifuging as before. The particles were finally suspended in UltraPure water (10 mL). Particle solution (2 mL) and UltraPure water (13 mL) were added to a pre-rinsed Centriprep Ultracel YM-50 spin filter (50,000 MWCO, Millipore) and centrifuged (1500 × *g*, room temperature, 30 min), and the particle-containing retentate was resuspended in 12 mL of UltraPure water. This wash step was repeated until the UV absorbance of the filtrate in the 200–350 nm range reached baseline values. The final retentate was serially passed through 0.2 μm PVDF (Pall) and 0.1 μm Anotop (Whatman) syringe filters and lyophilized overnight to yield a fluffy, orange powder.

Nanoparticles without Arg_9 incorporated into the polymer structure were prepared as described above, with the exception that the monomer solution consisted of acrylamide (62.5 mg, 879 μmol), N,N'-methylene-bis-acrylamide (7.20 mg, 46.7 μmol), and N-acryloyltyramine (1.80 mg, 9.41 μmol), and omitted the Arg_9.

Synthesis of Polyacrylamide Microparticles (PMP)

PMP encapsulating BSA-488 and either not modified or modified with Arg_9 (Figure 1) were synthesized as described previously.[12]

Scanning Electron Microscopy (SEM)

Particle samples were prepared as described previously[12, 13] and imaged using a Hitachi S-5000 SEM at 10 kV.

Particle Size and Zeta-potential Measurements

he size distributions of particles suspended at 0.1 mg/mL in PBS were determined by light scattering using a Zetasizer Nano-ZS (Malvern Instruments) for PNP, or a Horiba Partica LA-950 for PMP, as described previously.[13] The zeta-potentials of particles suspended in UltraPure water (PNP, 4 mg/mL and PMP, 0.5 mg/mL) were measured using a Zetasizer Nano-ZS at 25°C.

Cell culture and in vitro particle uptake assay

The transformed human bronchial epithelial cell line BEAS 2B (CRL-9609, ATCC, Manassas, VA) was cultured in DMEM supplemented with 10% fetal calf serum and antibiotics. For studies with particles, 2×10^5 cells were incubated with 5 μg/mL of PMP (CPP− or CPP+) or 10 μg/mL of PNP (CPP− or CPP+) that were freshly sonicated. After 24 h, cell layers were washed 3 times with PBS and the percentage of cells containing BSA-488 was quantified by flow cytometry as described below.

Radionuclide preparation

Carrier-free ^{125}I radionuclide was purchased from Perkin Elmer. ^{76}Br was produced at the Washington University cyclotron facility by the ^{76}Se (p,n) ^{76}Br nuclear reaction on a ^{76}Se-enriched Cu_2Se target. ^{76}Br was recovered by a modified dry distillation method,[28] filtered through a C-18 Sep-Pak light cartridge (Waters Corp.), dried under nitrogen gas, then reconstituted in water (Milli-Q, Millipore) immediately before use. Labeling efficiency and radiochemical purity of labeled particles was determined by radio-thin layer chromatography (radio-TLC, Bioscan System 2000).

Particle radiolabeling

For bio-distribution studies, particles were labeled with ^{125}I using an iodination protocol modified from Markwell.[29] All particles were labeled using the tyrosine residues of the encapsulated BSA-488 while the PNP were additionally labeled on the tyramine residues of the polymer backbone. To achieve this, 500 μg of lyophilized particles were reconstituted in 250 μL PBS, sonicated for 5 min (Branson 1510) and mixed with 300 μCi of ^{125}I in 10 μL of diluted NaOH solution as described.[29] The reaction was then incubated at room temperature for 30 min and monitored by radio-TLC. The radio-iodinated PMP particles were purified by centrifugation at 5000*g* for 10 min to remove free ^{125}I. ^{125}I-labeled PNP particles were precipitated with absolute ethanol then collected by repeated centrifugation. For positron emission tomography (PET) imaging, particles were labeled with ^{76}Br using a previously described approach.[4] The final radiochemical purity of all particles was greater than 95%. The in vitro stability of radiolabeled particles was determined by monitoring radio-TLC after

incubation with mouse serum (Sigma-Aldrich) at 37°C (data not shown). Particles were diluted with PBS to a final concentration of 100 μg/50 μL for administration to mice.

Mice and particle delivery

C57BL/6J mice were obtained from Jackson Laboratory and housed under pathogen-free conditions. The Animal Studies Committee of the Washington University School of Medicine approved all protocols. Mice were anesthetized with intraperitoneal Avertin, 200 mg/kg, prior to neck dissection for cannulation of the trachea with a 22-gauge angiocatheter. For intratracheal delivery, PBS alone or particles (100 μg/50 μL) in PBS followed by 50 μL of air as dead space was administered through the catheter as a single bolus.

Small animal microPET imaging

Anesthetized mice (n=3–5 per group) were administered 10–20 μCi of 100 μg ^{76}Br-labeled particles in 50 μL PBS by intratracheal injection. Imaging was performed 1, 3 and 18 h post-injection using a static 30 min frame with a microPET Focus 120 or 220 scanner, which have the same resolution (Siemens Medical Solutions).30 X-ray computed tomography (CT) imaging (15 min frame) was performed immediately following acquisition of PET images using a MicroCAT II instrument (CTI-Imtek).31 The microPET and CT images were co-registered using fiduciary markers attached to the animal positioning bed and quantitatively analyzed using AMIRA software (Mercury Computer Systems). Data were calculated as standardized uptake values (SUVs) within lung fields identified by the CT images and calculated using a lung tissue density of 0.3g/mL. The SUV numbers were calculated in multiple 3-dimensional regions of interest within the lung fields as described.32

Biodistribution studies

Anesthetized mice were injected intratracheally with 1 μCi of 100 μg ^{125}Ilabeled particles in 50 μL PBS. At 1, 3, and 24 h post-injection, the mice were euthanized by CO_2 asphyxiation and organs of interest were collected for determination of activity using a Beckman Gamma counter 8000. For analysis of lung bronchoalveolar lavage, the trachea was cannulated and lavaged three times with 1 mL aliquots of PBS. A dilution of the administered dose of ^{125}I-labeled particles (1:100 dilution) was counted in parallel with the organ samples to calculate the percentage of activity relative to the instilled dose per organ (%ID/organ) as previously described.[33] All data were corrected for radioactive decay of ^{125}I.

Bronchoalveolar lavage (BAL) and lung tissue samples

Lungs were subjected to BAL with 1 mL of PBS. BAL fluid was centrifuged and the cell-free supernatant was collected and stored for cytokine analysis, while the cell pellet was resuspended in 1 mL of PBS for total cell count, cytospin preparation, flow cytometry or alveolar macrophage culture. The immune cell differential was determined using standard light microscopy criteria as described previously.[34] Following BAL, lungs were inflated with 1 mL of cryopreservation media (Tissue-tek), frozen on dry ice and stored at −80 °C prior to sectioning.

Flow cytometry

Cell lines or cells collected by BAL were washed twice with flow cytometry buffer (PBS with 2% FBS). BAL cells were blocked using purified rat anti-mouse CD16/CD32 (Mouse BD Fc Block, BD Biosciences) and then immunostained with macrophage marker rat anti-mouse F4/80 (Serotec) or with IgG2b isotype control antibody, both conjugated with APC. Cells were again washed twice with FACS buffer and analyzed on a FACSCalibur flow cytometer (10,000 events per sample) using CELLquest software (BD Biosciences).

Immunostaining and microscopy

Frozen tissue sections and BAL cytospin preparations were fixed with 4% paraformaldehyde in PBS for 10 min at room temperature. Primary antibodies (and dilutions) used were rabbit anti-prosurfactant protein C (1:1000, Abcam) and biotinylated anti-CD68 (dilution 1:75, Serotec). Antibody binding was detected using secondary antibodies conjugated with Alexa Fluor dyes (Invitrogen) or streptavidin, and nuclei were stained with 4',6'-diamidino-2-phenylindole (DAPI; Vector Laboratories). Images were captured using a Leica DM5000 microscope (Wetzlar, Germany) with a Retiga 200R charge-coupled device camera interfaced with QCapture Pro software (Q Imaging). Fluorescence and differential interference contrast images were overlaid in QCapture Pro. Images were composed using Photoshop and Illustrator software (Adobe Systems).

Cytokine assays

To quantify inflammatory mediators in cell-free BAL fluid from mice following administration of particles, supernatants were analyzed in a multiplex, flow cytometry-based assay according to the manufacturer's protocol (BioPlex, Bio-Rad). Unique beads conjugated with a distinct capture antibody were incubated with 50 μL of BAL and 0.5% BSA or a serially diluted standard mix with a known concentration of all measured inflammatory mediators and compared to the standard curves as previously described.[34]

Statistical analysis

Groups were compared with Student’s t-test or one-way ANOVA and Scheffé post-testing performed using SPSS statistical software. The level of significance was set at $p < 0.05$.

RESULTS

Synthesis and characterization of hydrogel particles

To explore the effects of carrier size and functionalization with a cell-penetrating peptide (CPP) on the behavior of hydrogel-based particles following intratracheal administration, we synthesized polyacrylamide microparticles (PMP) and nanoparticles (PNP) that were not (CPP −) or were (CPP+) co-polymerized with a monomer containing pendant nona-arginine peptide (Arg_9) (Figure 1A). While these particles can be synthesized to hydrolyze and release their cargo,[12] non-degradable particles were used in this study to enable the tracking of particle fate. All particles encapsulated a conjugate of bovine serum albumin and Alexa Fluor 488 dye (BSA-488) for fluorescence-based assays and for tyrosine radiolabeling. PNP radiolabel stability was improved by co-polymerizing a tyramine-functionalized monomer into the particle structure, in addition to thoroughly washing the particles using ultrafiltration. In the dry state, particles had a spherical shape when imaged by SEM (Figure 1B, C). When hydrated, the PMP were 1 to 5 μm and PNP 20 to 40 nm in diameter, as measured by light scattering (Table 1). The surface charge of the particles, as indicated by zeta-potential measurements, was positive, with the exception of the PMP CPP− particles, which were near neutral. We previously demonstrated preferential uptake of the PMP CPP+ compared to PMP CPP− particles in cell lines,[12] and thus extended these studies to evaluate the PNP in parallel with PMP (Figure 1D). The addition of the Arg_9 into the structure of both PMP and PNP particles significantly enhanced their cell uptake in vitro ($p<0.05$).

In vivo PET/CT imaging of radiolabeled nanoparticles following intratracheal delivery

As an initial evaluation of the in vivo behavior of PMP and PNP in the lung, particles were hydrated, radiolabeled with ^{76}Br for PET imaging. To ensure accurate lung delivery, particles were administered to mice by intratracheal (IT) injection. Radiolabeled IT particles were well tolerated without animal distress or mortality. Mice were imaged serially by whole body

microPET/CT scanning over an 18 h period (Figure 2A). For all particles at all time points, the microPET/CT co-registered images clearly showed a general restriction of the particles to the lung. Particles present in the gastrointestinal (GI) tract post-delivery were best revealed in three-dimensional reconstructions of the images obtained after 3 h. Based on these studies, the PNP had a more prolonged retention in the lung relative to the PMP (Figure 2B).

Image analysis using the standardized uptake values (SUV) of the two types of PMP showed that the lung activity of each particle decreased at a similar rate over time, but mice administered the PMP CPP+ particles had 34–50% lower lung activity than those receiving PMP CPP− particles (Figure 2C). Both PNP types displayed higher lung activity compared to each of the PMP forms. In addition, the PNP had a similar and constant lung signal over 18 h that appeared to be independent of the Arg_9 peptide. Collectively, this initial analysis demonstrated a consistent behavior related to size; the larger PMP were rapidly cleared, likely through mucociliary clearance to the GI tract, while the smaller PNP had sustained lung retention.

In vivo lung retention and biodistribution of particles following intratracheal delivery

To more precisely quantify the lung retention and fate of particles, biodistribution studies were performed in mice after IT delivery of ^{125}I-labeled particles. Retention of particles in the lung was determined by measuring activity in total lung tissue. Evaluation of all four types of particles again demonstrated that the majority of the initial activity was localized in the lung (Figure 3). Consistent with the PET images, the activity of the smaller particles (PNP) in the lung was both higher and more persistent than that of the larger ones (PMP). However, in this more sensitive assay, an effect of the CPP was observed, but differed for the two sizes of particles. For PMP, the presence of the CPP resulted in a lower lung retention profile at all times ($p<0.05$). The pattern was reversed in the case of the PNP, where the presence of the CPP resulted in significantly higher lung retention at all time points ($p<0.05$).

Studies by other groups have demonstrated that following respiratory tract administration, particles could be cleared from the lung to either the GI tract by mucociliary activity (after particles are swallowed in the posterior pharynx) or to the systemic circulation by transit from the air space through the alveolar epithelium-capillary endothelial barrier.27 To analyze extra-pulmonary particle fate, organs of interest were collected and activity quantified using a gamma counter. These biodistribution studies showed higher activity of PMP than PNP in the GI tract (stomach and intestines; 1 and 3 h; $p< 0.05$), suggesting rapid mucociliary clearance of the larger particles from the lung. Also, the blood clearance of the PMP was higher than that of the PNP at all time points, suggesting movement from the alveolar air space to the systemic circulation ($p< 0.05$). For all particles, activity was extremely low or undetectable in all other organs assayed. The possibility of central nervous system uptake was also determined, which we anticipated would be minimal as IT delivery avoids passage from the olfactory epithelium to the brain.35 For all particle types, activity was not detected in the brains isolated from mice after PET imaging (data not shown). Together, these biodistribution studies were consistent with the PET imaging studies, confirming rapid GI tract clearance of the PMP and a high specificity of lung retention of PNP that was significantly enhanced by the addition of Arg_9 ($p<0.05$).

Localization of intracellular targeting of polyacrylamide particles in vivo

Prior studies of particle modification have indicated that changes in surface characteristics as imparted by the addition of a polyarginine peptide may significantly alter predicted pathways.[36, 37] To define features of lung retention and particle fate, an additional cohort of animals was intratracheally administered ^{125}I-labeled particles and then subjected to bronchoalveolar lavage (BAL) at 1, 3, or 24 h post delivery (Figure 4A). Radioactivity in the BAL fluid and the post-BAL lung was determined to quantify particles in different lung compartments with

the knowledge that the BAL fluid would contain both free and immune cell-associated particles, while the post-BAL lung would additionally include parenchymal cell-associated particles. Consistent with the studies above, analysis of BAL fluid and remaining activity in the lung revealed that a greater fraction of PNP than PMP was retained in the lung. There was no significant difference in post BAL lung activity imparted by addition of CPP to the PMP ($p>0.05$). In contrast, at all time points, PNP CPP+ were retained at higher levels in the post-BAL lung than PNP CPP− ($p<0.05$) suggesting that the addition of the Arg_9 enhanced the association of the smaller nanoparticle within the lung parenchymal compartment.

To identify the specific cell types in the lung taking up the particles, tissue sections of lung were examined for colocalization of the BSA-488-labeled particles with cell-specific markers. Low power examination of lung sections showed that delivery of all particle types resulted in regional dispersal, variable clumping of particles and delivery within alveolar airspaces, which in some cases associated with cell surfaces (Figure 4B and data not shown). No significant particle fluorescence activity was identified in the airway epithelial cells of bronchi or bronchioles of any of the animals. All particle types were found in alveolar epithelial cells (Figure 4B, arrowheads). These were identified by morphology as alveolar epithelial type I cells or by immunostaining as type II cells using the marker prosurfactant protein C. Particles were more commonly observed within cells of macrophage morphology (Figure 4B, arrows). Consistent with this observation, BAL cells obtained 24 h post-instillation revealed particles in cells that expressed the macrophage marker CD68 (Figure 4C). These studies suggested that there was enhanced alveolar macrophage uptake of PNP compared to PMP particles.

Quantification of particle uptake by BAL alveolar macrophages in vivo

Optimal particle diameters for phagocytosis by alveolar macrophages are reported to be 1–3 μm, and phagocytosis is considered to decrease with particle size and time after delivery to the lung.[38, 39] To more specifically quantify alveolar macrophage uptake, we examined BAL cells from different time points after IT delivery using flow cytometry. Rapid uptake was observed for all particle types in 30–60% of the macrophages in samples obtained 3 h post-delivery (Figure 4D). By 24 h, there was a decrease in the percentage of macrophages containing PMP, while macrophage uptake of the PNP remained high (>50%). There was no apparent effect of CPP to augment macrophage uptake of either particle.

Determination of the acute inflammatory cell response in the lung after delivery of particles

The respiratory system response to particulate invasion is typically accompanied by a rapid inflammatory response that can be monitored by assay of immune cells and accompanying inflammatory mediators in BAL fluid.[34, 40] Few studies have explored responses to synthetic particles specifically developed for nanomedicine.[10, 41, 42] It was therefore important to next determine if there was a toxic inflammatory response in the lung following IT delivery of particles (Figure 5A). Cells in BAL fluid recovered from naive mice include at least 95% alveolar macrophages, reflecting the normal innate cell population. After 24 h, PMP CPP−, PNP CPP− or PNP CPP+ particles did not induce a significant change in the number or type of immune cells recovered compared to PBS alone (Figure 5B). Only the PMP CPP+ particles induced an inflammatory response characterized by an increase in BAL fluid neutrophils and a decrease in macrophages. This could not be directly attributed to the Arg_9 since there was no inflammatory response observed in BAL fluid of mice delivered purified Arg_9 peptide alone (Figure 5C). In agreement with the inflammatory cell profiles in the BAL fluid, further analysis that quantified multiple cytokines, chemokines and growth factors in cell-free BAL fluid showed increased levels only in samples from mice administered PMP CPP+ (Figure 5D). The inflammatory mediators with increased concentrations were CXCL1/KC, CCL2/JE, CCL3/MIP-1α and G-CSF, consistent with the function of these molecules as neutrophil chemotaxis

factors.[40] Taken together, our in vivo analysis reveals that both size and functionalization impart each type of particle with its own unique behavior (Table 2).

DISCUSSION

The use of custom engineered and functionalized nanoparticles provides significant possibilities for improving diagnostic imaging and unique therapies for lung disease. However, development of these tools for human applications demands comprehensive in vivo assessment. In this study, tracking of particle fate is made possible by the ability to multi-functionalize our particle system, reflecting one advantage of these synthetic polymer constructs. Here, we show that the direct and commonly used clinical route of respiratory tract delivery for administration of our polymer based micro- and nanoparticles results in reproducible behaviors for adaptation to imaging and therapeutic applications in the lung (Table 2). We also specifically tested the functionalization of particles with CPP since it is remarkably effective for cargo delivery in vitro and in some cases when delivered intravenously.[20–22] To our knowledge, nanoparticles bearing CPPs have not been previously studied for delivery to the respiratory tract, where cell targets and host defense mechanisms present an environment that is very different than that of the vascular system and other organs. We identified that the addition of the Arg_9 CPP to the carrier structure induced significant changes in particle behavior in vivo, particularly enhancing lung airspace retention of the PNP without induction of inflammation when delivered to the respiratory tract of mice.

Our multi-modality analysis of the acute behavior of CPP functionalized micro- and nano-sized particles delivered intratracheally also revealed important findings with direct implications for particle design for clinical applications. First, PET imaging showed that both large and small particle types were distributed widely throughout lung airspaces, independent of the presence of CPP and any differences in surface charge. By labeling the particles with multiple markers, we could use whole animal, tissue and cell-based analysis to determine that the PET imaging correlated well with airspace filling and mucociliary clearance. Second, using these assays, we confirmed that the routes of particle clearance were size-dependent as reported by others: the larger particles (PMP) were more rapidly cleared by mucociliary mechanisms, likely due to a tendency for more proximal impaction in the airway of respiratory tract.[36, 39] Consistent with this conclusion, the biodistribution assay (Figure 3) revealed significantly higher PMP than PNP GI tract activity at one and three hours post-delivery ($p<0.05$). This is the result of movement of particles (or particles within cells), up the mucociliary escalator and subsequent swallowing. Thus lower mucociliary clearance contributed to the prolonged lung retention of PNP. Size-dependent behavior related to transit to the blood was opposite of that predicted, based on prior reports.[27, 43] These reports indicated that a significant proportion of nanoparticles transit the alveolar space to the blood. In contrast, we found a greater fraction of PMP in the blood pool, possibly owing to some unrecognized alteration or injury to the alveolar epithelial cell basement membrane.27 Third, both large and small particles were rapidly taken up by alveolar macrophages, without enhancement of phagocytosis by CPP. For PNP in particular, macrophage uptake is thus likely the major route for clearance, whereas it is possible that a high proportion of PMP clearance is by mucociliary routes without phagocytosis. The relatively greater macrophage uptake of nanoparticles than microparticles may also be the result of a higher amount of PNP than PMP delivered since dosing was based on mass. Fourth, epithelial cell uptake was independent of the addition of the Arg_9 CPP for both sizes of particles, as opposed to the enhanced uptake that we observed in vitro.[12] Last, in contrast to reports of inflammation induced by other particles,[10, 36] acute airway inflammation, assessed at 24 h after delivery was not induced, with the single exception of the PMP CPP+.

We found that the presence of Arg_9 significantly alters the behavior of the particles in the lung. Interestingly, Arg_9 improves the lung retention of the PNP, while it speeds up clearance of the

larger PMP. The prolonged retention of the PNP with Arg_9 could not be attributed to the difference in charge alone since both PMP CPP+ and PNP CPP+ were of similar surface charge (Table 1). These differences in behavior caused by a small perturbation to the carrier structure highlight the need to take into account multi-level (cell, organ, and whole organism) effects in the design of particle-based carrier systems. Prior studies of respiratory tract delivery of CPP −bearing molecules are limited and have mixed results, indicating that multiple design features must be considered. For example, IT delivery of luciferase plasmid with a TAT-derived CPP linked via a polyethylene glycol (PEG) bridge to polyethylenimine, did result in a low level of total lung luciferase expression.[25] However, in that report, Kleeman et al. argued that TAT-derived peptide alone was insufficient to mediate in vivo transfection of lung cells and that the PEG conjugate was a critical component for delivery. Other investigators have suggested that the addition of hydrophilic PEG may be a critical factor for enhancing penetration of particles through the dense, thin mucous layer that normally lines the respiratory tract.[44, 45] It is possible that the use of a PEG linker incorporated into our hydrogel particles could permit the CPP to function more effectively in vivo. On the other hand, the nanoparticles that contact the alveolar epithelial cells face a high surfactant barrier, where additional particle surface properties may need to be engineered to enable cell entry. Additional factors, such as particle shape and charge are likely also important to maximize CPP-mediated nanoparticle uptake and represent areas for future investigation to optimize lung delivery.[46]

We also investigated the lung inflammatory responses of our particles using both quantification of immune cells recovered in BAL fluid and cytokines in cell-free BAL. We found that 24 h following tracheal instillation, only the PMP CPP+ induced increased numbers of neutrophils in the BAL fluid. In contrast, the PMP CPP− or the Arg_9 peptide alone did not increase neutrophils, suggesting that the presence of the cationic Arg_9 in the context of the PMP structure may have enhanced toxicity. This is analogous to the lung inflammation observed when TAT peptides were linked to different types of siRNA or DNA resulting in the induction of inflammation in the lung.[25, 26] As noted, the surface charge of the PMP CPP+ was similar to the relatively non-inflammatory PNP CPP+, again indicating that combinations of size, charge and other particle design features may influence the development of inflammation. The inflammatory response induced by PMP CPP+ was accompanied by increased levels of chemokines and growth factors that are known to enhance neutrophil influx in the lung (e.g., CXCL1, CCL2, CCL3, G-CSF).[40] The source of this inflammation may be the result of an interaction of peptide-bearing particles with alveolar macrophages, or airway or alveolar epithelial cells as reported.[47, 48] However, when we exposed primary alveolar macrophages to particles and measured cytokines in supernatants, we did not observe an increase in cytokine or chemokine production (data not shown), in contrast to macrophage responses observed by others.[48] We further recognized that the present experiments were designed to study only an acute effect where prolonged retention of particles may induce a chronic response as observed in the case of intratracheally administered carbon nanotubes.[49]

Although we used several assays to determine the fate and effects of intratracheal delivery of our particles, elucidating additional aspects of particle behavior will require future investigation. For example, we need to gain further insight into the mechanisms for prolonged retention of the PNP nanoparticle and facilitation by Arg_9. While retention could be strongly influenced by particle biodegradability, it may also be associated with particle size, shape and surface charge. We have also considered that retention may be related to the movement of particles to the alveolar interstitial space, a phenomenon observed in the study of ultrafine particles.[38] However, using immunofluorescence microscopy, we did not observe BSA-488-labeled particles within the interstitial space of the alveoli. The use of immunogold-labeled anti-Alexa Fluor 488 antibodies and electron microscopy of lung tissues analyzed over a longer period of time might reveal this behavior. Also, while the mechanism of uptake of a variety of structures with CPP has been extensively investigated,[20–22] it is possible that unique pathways

independent of CPP might exist for the polyacrylamide complexes tested here, possibly related to their inherently hydrophilic nature. Future assessment of particles functionalized with CPP will be directed toward testing designs that incorporate fully biodegradable components50 and the addition of PEG to enhance mucous penetration,[44] as well as investigating lung retention beyond 24 hours. The encapsulation of a biologically active cargo within the particle that results in the expression of a biologic or molecular marker (e.g., green fluorescent protein) or a therapeutic molecule will further enhance our ability to assess the value of nanoparticle systems for diagnostic and therapeutic applications.

CONCLUSION

Synthetic polymer-based hydrogel particles provide the flexibility required to incorporate targeting peptides and imaging probes, plus package diagnostic and therapeutic cargoes for delivery to the lung. Examination of the fate of model particles labeled to enable tracking show that changes in size, charge and functionalization result in unique behaviors, each with clinical implications. The larger PMP are briefly retained throughout the airspaces, then cleared rapidly by the GI tract (likely via mucociliary routes), and have a short lung half-life. In the absence of the CPP Arg_9, these particles did not induce acute inflammation and thus could be used for diagnostic imaging or delivery that require relatively brief lung dwell times such as for acute lung injury (e.g., acute lung infection and acute respiratory distress syndrome). In contrast, the smaller PNP have a higher and more prolonged lung airspace retention, which is further augmented by Arg_9 without acute lung inflammation. These nanoparticles may be more advantageous for serial imaging or therapy of a more persistent lung injury. The high and prolonged uptake of particles in macrophages could be capitalized on for treatment of slow growing and difficult to treat intracellular microorganisms such as mycobacterium tuberculosis, as suggested by others.[8,11,51] Enhanced release of anti-tuberculosis agents using microparticles and nanoparticle constructs have been considered based on the potential to reduce systemic toxicity, provide higher local concentrations of drug, and thereby reduce dose frequency compared to current oral drugs.[8,11,51] Clinical delivery of nanoparticles to the lung may be facilitated by existing aerosolize devises that can be used to generate mist for impaction in airways or alveolar spaces.[11,38] As we demonstrate, functionalization of our particle systems with these or other diagnostic and therapeutic agents may further alter the material characteristics of the carrier (e.g., surface charge, size, etc.), which will continue to drive the need for comprehensive in vivo characterization of particle behavior.

Supplementary Material

Refer to Web version on PubMed Central for supplementary material.

Abbreviations

Arg_9	nona-arginine
BAL	bronchoalveolar lavage
BSA	bovine serum albumin
CPP	cell penetrating peptide
CT	computed tomography
DAPI	4',6'-diamidino-2-phenylindole
GI	gastrointestinal
PBS	phosphate buffered saline

PET	positron emission tomography
PEG	polyethylene glycol
PMP	polyacrylamide microparticles
PNP	polyacrylamide nanoparticles
SEM	scanning electron microscopy
SPC	prosurfactant protein C
SUV	standardized uptake values
TAT	trans-activator of transcription
TLC	thin layer chromatography

Acknowledgments

We thank Matt Bernstein for assistance with initial in vivo studies, Nicole Fettig, Terry Sharp, Amanda Roth, Margaret Morris, Jerrel Rutlin, Lori Strong, Ann Stoncek and James Kozlowski for assistance with biodistribution and imaging studies, and Cassandra Mikols for Bioplex assays. This work was supported by awards from the National Institutes of Health, including the NHLBI Program of Excellence in Nanotechnology (UO1 HL080729), NBIB grant R01-EB005824 for particle design, and NIH CA86307 for the production of ^{64}Cu and ^{76}Br, and the Children's Discovery Institute of St. Louis Children's Hospital and Washington University for the work performed by the Respiratory Cell Culture Core.

LITERATURE CITED

1. Sajja HK, East MP, Mao H, Wang YA, Nie S, Yang L. Development of multifunctional nanoparticles for targeted drug delivery and noninvasive imaging of therapeutic effect. Curr. Drug Discov. Technol 2009;6(1):43–51. [PubMed: 19275541]
2. Balazs AC, Emrick T, Russell TP. Nanoparticle polymer composites: where two small worlds meet. Science 2006;314(5802):1107–1110. [PubMed: 17110567]
3. Wooley KL, Moore JS, Wu C, Yang Y. Novel polymers: molecular to nanoscale order in three dimensions. Proc. Natl. Acad. Sci. U. S. A 2000;97(21):11147–11148. [PubMed: 11027324]
4. Almutairi A, Rossin R, Shokeen M, Hagooly A, Ananth A, Capoccia B, Guillaudeu S, Abendschein D, Anderson CJ, Welch MJ, Frechet JM. Biodegradable dendritic positron-emitting nanoprobes for the noninvasive imaging of angiogenesis. Proc. Natl. Acad. Sci. U. S. A 2009;106(3):685–690. [PubMed: 19129498]
5. Lee CC, Gillies ER, Fox ME, Guillaudeu SJ, Frechet JM, Dy EE, Szoka FC. A single dose of doxorubicin-functionalized bow-tie dendrimer cures mice bearing C-26 colon carcinomas. Proc. Natl. Acad. Sci. U. S. A 2006;103(45):16649–16654. [PubMed: 17075050]
6. Kumar M, Behera AK, Lockey RF, Zhang J, Bhullar G, De La Cruz CP, Chen LC, Leong KW, Huang SK, Mohapatra SS. Intranasal gene transfer by chitosan-DNA nanospheres protects BALB/c mice against acute respiratory syncytial virus infection. Hum. Gene Ther 2002;13(12):1415–1425. [PubMed: 12215263]
7. Gelperina S, Kisich K, Iseman MD, Heifets L. The potential advantages of nanoparticle drug delivery systems in chemotherapy of tuberculosis. Am. J. Respir. Crit. Care Med 2005;172(12):1487–1490. [PubMed: 16151040]
8. Azarmi S, Roa WH, Lobenberg R. Targeted delivery of nanoparticles for the treatment of lung diseases. Adv. Drug Deliv. Rev 2008;60(8):863–875. [PubMed: 18308418]
9. Yokohira M, Kuno T, Yamakawa K, Hosokawa K, Matsuda Y, Hashimoto N, Suzuki S, Saoo K, Imaida K. Lung toxicity of 16 fine particles on intratracheal instillation in a bioassay model using f344 male rats. Toxicol. Pathol 2008;36(4):620–631. [PubMed: 18467675]

10. Muhlfeld C, Rothen-Rutishauser B, Blank F, Vanhecke D, Ochs M, Gehr P. Interactions of nanoparticles with pulmonary structures and cellular responses. Am. J. Physiol. Lung Cell Mol. Physiol 2008;294(5):L817–L829. [PubMed: 18263666]
11. Sung JC, Pulliam BL, Edwards DA. Nanoparticles for drug delivery to the lungs. Trends Biotechnol 2007;25(12):563–570. [PubMed: 17997181]
12. Cohen JL, Almutairi A, Cohen JA, Bernstein M, Brody SL, Schuster DP, Frechet JM. Enhanced cell penetration of acid-degradable particles functionalized with cell-penetrating peptides. Bioconjug. Chem 2008;19(4):876–881. [PubMed: 18318462]
13. Cohen JA, Beaudette TT, Tseng WW, Bachelder EM, Mende I, Engleman EG, Frechet JM. T-cell activation by antigen-loaded pH-sensitive hydrogel particles in vivo: the effect of particle size. Bioconjug. Chem 2009;20(1):111–119. [PubMed: 19102625]
14. Murthy N, Thng YX, Schuck S, Xu MC, Frechet JM. A novel strategy for encapsulation and release of proteins: hydrogels and microgels with acid-labile acetal cross-linkers. J. Am. Chem. Soc 2002;124 (42):12398–12399. [PubMed: 12381166]
15. Murthy N, Xu M, Schuck S, Kunisawa J, Shastri N, Frechet JM. A macromolecular delivery vehicle for protein-based vaccines: acid-degradable protein-loaded microgels. Proc. Natl. Acad. Sci. U. S. A 2003;100(9):4995–5000. [PubMed: 12704236]
16. Goh SL, Murthy N, Xu M, Frechet JM. Cross-linked microparticles as carriers for the delivery of plasmid DNA for vaccine development. Bioconjug. Chem 2004;15(3):467–474. [PubMed: 15149173]
17. Bartlett DW, Su H, Hildebrandt IJ, Weber WA, Davis ME. Impact of tumor-specific targeting on the biodistribution and efficacy of siRNA nanoparticles measured by multimodality in vivo imaging. Proc. Natl. Acad. Sci. U. S. A 2007;104(39):15549–15554. [PubMed: 17875985]
18. Yamamoto H, Kuno Y, Sugimoto S, Takeuchi H, Kawashima Y. Surface-modified PLGA nanosphere with chitosan improved pulmonary delivery of calcitonin by mucoadhesion and opening of the intercellular tight junctions. J. Control. Release 2005;102(2):373–381. [PubMed: 15653158]
19. Frankel AD, Pabo CO. Cellular uptake of the tat protein from human immunodeficiency virus. Cell 1988;55(6):1189–1193. [PubMed: 2849510]
20. Snyder EL, Dowdy SF. Cell penetrating peptides in drug delivery. Pharm. Res 2004;21(3):389–393. [PubMed: 15070086]
21. Vives E, Schmidt J, Pelegrin A. Cell-penetrating and cell-targeting peptides in drug delivery. Biochim. Biophys. Acta 2008;1786(2):126–138. [PubMed: 18440319]
22. Stewart KM, Horton KL, Kelley SO. Cell-penetrating peptides as delivery vehicles for biology and medicine. Org. Biomol. Chem 2008;6(13):2242–2255. [PubMed: 18563254]
23. Fawell S, Seery J, Daikh Y, Moore C, Chen LL, Pepinsky B, Barsoum J. Tat-mediated delivery of heterologous proteins into cells. Proc. Natl. Acad. Sci. U. S. A 1994;91(2):664–668. [PubMed: 8290579]
24. Schwarze SR, Ho A, Vocero-Akbani A, Dowdy SF. In vivo protein transduction: delivery of a biologically active protein into the mouse. Science 1999;285(5433):1569–1572. [PubMed: 10477521]
25. Kleemann E, Neu M, Jekel N, Fink L, Schmehl T, Gessler T, Seeger W, Kissel T. Nano-carriers for DNA delivery to the lung based upon a TAT-derived peptide covalently coupled to PEG-PEI. J. Control. Release 2005;109(1–3):299–316. [PubMed: 16298009]
26. Moschos SA, Jones SW, Perry MM, Williams AE, Erjefalt JS, Turner JJ, Barnes PJ, Sproat BS, Gait MJ, Lindsay MA. Lung delivery studies using siRNA conjugated to TAT(48–60) and penetratin reveal peptide induced reduction in gene expression and induction of innate immunity. Bioconjug. Chem 2007;18(5):1450–1459. [PubMed: 17711319]
27. Shimada A, Kawamura N, Okajima M, Kaewamatawong T, Inoue H, Morita T. Translocation pathway of the intratracheally instilled ultrafine particles from the lung into the blood circulation in the mouse. Toxicol. Pathol 2006;34(7):949–957. [PubMed: 17178695]
28. Tolmachev V, Lundqvist H, Einarsson L. Production of 61Cu from a natural nickel target. Appl. Radiat. Isot 1998;49(1–2):79–81. [PubMed: 9467838]

29. Markwell MA, Fox CF. Surface-specific iodination of membrane proteins of viruses and eucaryotic cells using 1,3,4,6-tetrachloro-3alpha,6alpha-diphenylglycoluril. Biochemistry 1978;17(22):4807–4817. [PubMed: 215191]
30. Tai YC, Ruangma A, Rowland D, Siegel S, Newport DF, Chow PL, Laforest R. Performance evaluation of the microPET focus: a third-generation microPET scanner dedicated to animal imaging. J. Nucl. Med 2005;46(3):455–463. [PubMed: 15750159]
31. Paulus MJ, Gleason SS, Kennel SJ, Hunsicker PR, Johnson DK. High resolution X-ray computed tomography: an emerging tool for small animal cancer research. Neoplasia 2000;2(1–2):62–70. [PubMed: 10933069]
32. Rossin R, Muro S, Welch MJ, Muzykantov VR, Schuster DP. In vivo imaging of 64Cu-labeled polymer nanoparticles targeted to the lung endothelium. J. Nucl. Med 2008;49(1):103–111. [PubMed: 18077519]
33. Edwards WB, Anderson CJ, Fields GB, Welch MJ. Evaluation of radiolabeled type IV collagen fragments as potential tumor imaging agents. Bioconjug. Chem 2001;12(6):1057–1065. [PubMed: 11716700]
34. Gunsten S, Mikols CL, Grayson MH, Schwendener RA, Agapov E, Tidwell RM, Cannon CL, Brody SL, Walter MJ. IL-12 p80-dependent macrophage recruitment primes the host for increased survival following a lethal respiratory viral infection. Immunology 2009;126(4):500–513. [PubMed: 18783467]
35. Oberdorster G, Sharp Z, Atudorei V, Elder A, Gelein R, Kreyling W, Cox C. Translocation of inhaled ultrafine particles to the brain. Inhal. Toxicol 2004;16(6–7):437–445. [PubMed: 15204759]
36. Rogueda PG, Traini D. The nanoscale in pulmonary delivery. Part 1: deposition, fate, toxicology and effects. Expert Opin. Drug Deliv 2007;4(6):595–606. [PubMed: 17970663]
37. Yang W, Peters JI, Williams RO 3rd. Inhaled nanoparticles--a current review. Int. J. Pharm 2008;356(1–2):239–247. [PubMed: 18358652]
38. Semmler-Behnke M, Takenaka S, Fertsch S, Wenk A, Seitz J, Mayer P, Oberdorster G, Kreyling WG. Efficient elimination of inhaled nanoparticles from the alveolar region: evidence for interstitial uptake and subsequent reentrainment onto airways epithelium. Environ. Health Perspect 2007;115(5):728–733. [PubMed: 17520060]
39. Geiser M, Casaulta M, Kupferschmid B, Schulz H, Semmler-Behnke M, Kreyling W. The role of macrophages in the clearance of inhaled ultrafine titanium dioxide particles. Am. J. Respir. Cell Mol. Biol 2008;38(3):371–376. [PubMed: 17947511]
40. Mizgerd JP. Molecular mechanisms of neutrophil recruitment elicited by bacteria in the lungs. Semin. Immunol 2002;14(2):123–132. [PubMed: 11978084]
41. De Jong WH, Borm PJ. Drug delivery and nanoparticles:applications and hazards. Int J Nanomedicine 2008;3(2):133–149. [PubMed: 18686775]
42. Dailey LA, Jekel N, Fink L, Gessler T, Schmehl T, Wittmar M, Kissel T, Seeger W. Investigation of the proinflammatory potential of biodegradable nanoparticle drug delivery systems in the lung. Toxicol. Appl. Pharmacol 2006;215(1):100–108. [PubMed: 16551473]
43. Nemmar A, Hoet PH, Vanquickenborne B, Dinsdale D, Thomeer M, Hoylaerts MF, Vanbilloen H, Mortelmans L, Nemery B. Passage of inhaled particles into the blood circulation in humans. Circulation 2002;105(4):411–414. [PubMed: 11815420]
44. Lai SK, Wang YY, Hanes J. Mucus-penetrating nanoparticles for drug and gene delivery to mucosal tissues. Adv. Drug Deliv. Rev 2009;61(2):158–171. [PubMed: 19133304]
45. Wang YY, Lai SK, Suk JS, Pace A, Cone R, Hanes J. Addressing the PEG mucoadhesivity paradox to engineer nanoparticles that "slip" through the human mucus barrier. Angew Chem. Int. Ed. Engl 2008;47(50):9726–9729. [PubMed: 18979480]
46. Zhang K, Fang H, Chen Z, Taylor JS, Wooley KL. Shape effects of nanoparticles conjugated with cell-penetrating peptides (HIV Tat PTD) on CHO cell uptake. Bioconjug. Chem 2008;19(9):1880–1887. [PubMed: 18690739]
47. Barlow PG, Clouter-Baker A, Donaldson K, Maccallum J, Stone V. Carbon black nanoparticles induce type II epithelial cells to release chemotaxins for alveolar macrophages. Part. Fibre Toxicol 2005;2:11. [PubMed: 16332254]

48. Bastus NG, Sanchez-Tillo E, Pujals S, Farrera C, Kogan MJ, Giralt E, Celada A, Lloberas J, Puntes V. Peptides conjugated to gold nanoparticles induce macrophage activation. Mol. Immunol 2009;46 (4):743–748. [PubMed: 18996597]

49. Lam CW, James JT, McCluskey R, Hunter RL. Pulmonary toxicity of single-wall carbon nanotubes in mice 7 and 90 days after intratracheal instillation. Toxicol. Sci 2004;77(1):126–134. [PubMed: 14514958]

50. Broaders KE, Cohen JA, Beaudette TT, Bachelder EM, Frechet JM. Acetalated dextran is a chemically and biologically tunable material for particulate immunotherapy. Proc. Natl. Acad. Sci. U. S. A 2009;106(14):5497–5502. [PubMed: 19321415]

51. Verma RK, Kaur J, Kumar K, Yadav AB, Misra A. Intracellular time course, pharmacokinetics, and biodistribution of isoniazid and rifabutin following pulmonary delivery of inhalable microparticles to mice. Antimicrob. Agents Chemother 2008;52(9):3195–3201. [PubMed: 18591268]

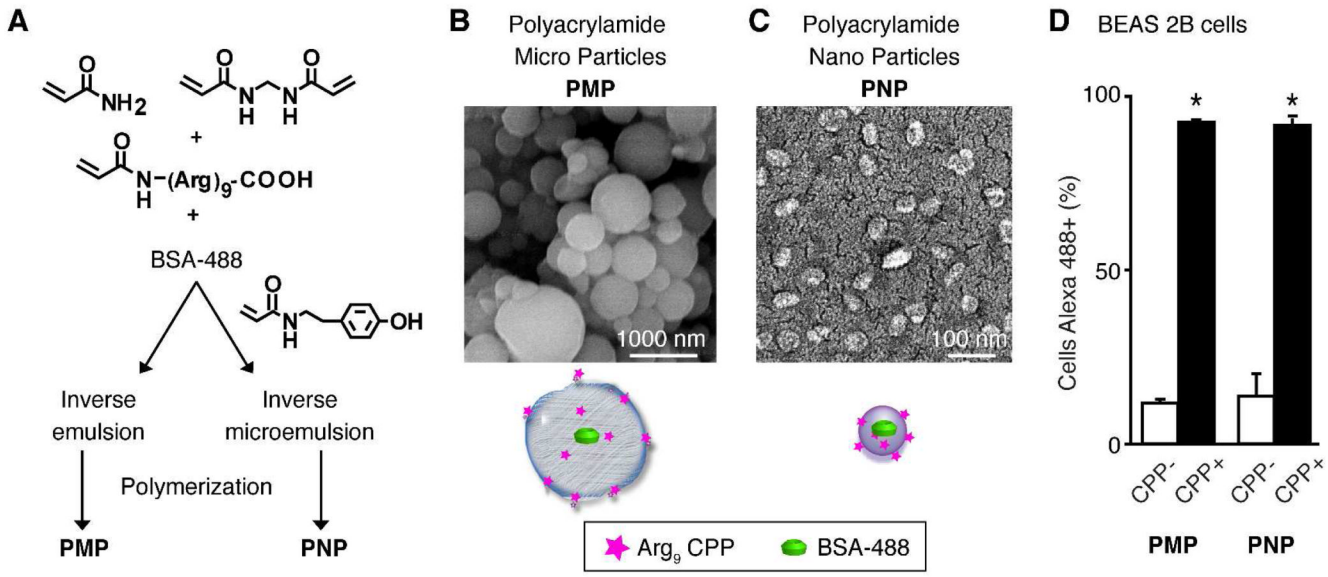

Figure 1.

Synthesis, functionalization, and in vitro behavior of polyacrylamide hydrogels. (A) Particles were generated and co-polymerized in the absence or presence of a nona-arginine cell-penetrating peptide (Arg_9). All particles encapsulated bovine serum albumin conjugated with Alexa Fluor 488 dye (BSA-488) for fluorescence detection. Emulsion conditions were varied to yield polyacrylamide microparticles (PMP) or nanoparticles (PNP) as shown in the SEM images (B, C) of the particles in the dry state. (D) The human bronchial epithelial cell line BEAS 2B was incubated with the indicated particles for 24 h then assayed by flow cytometry to determine the proportion of cells containing BSA-488-labeled particles. Shown is the mean ± S.D. of replicate samples from at least 2 independent experiments (*$p<0.05$). 145×69mm (600 × 600 DPI)

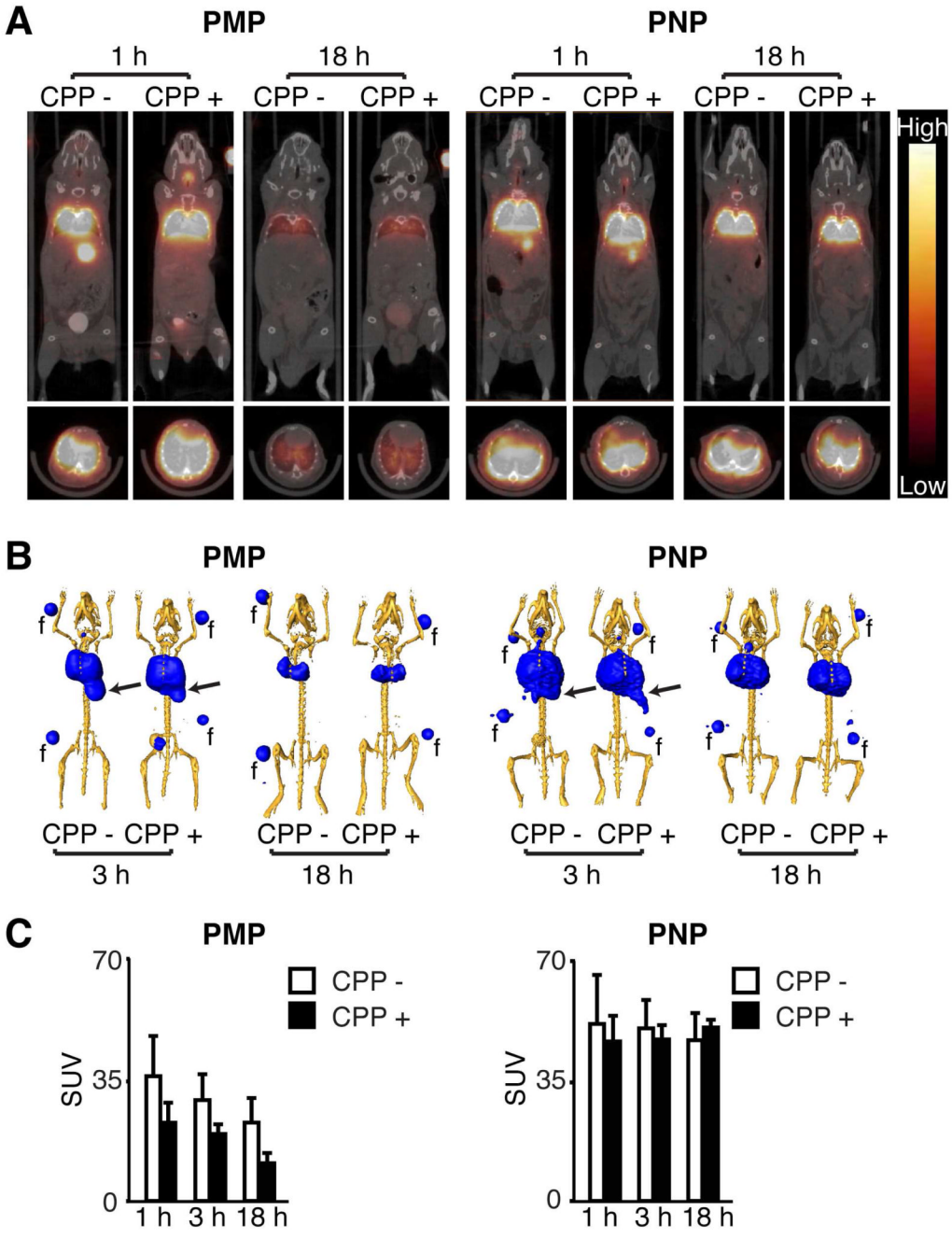

Figure 2.

MicroPET/CT imaging of ^{76}Br-labeled particles following intratracheal delivery. (A) Representative mid-thoracic coronal (top) and transverse (bottom) slices of serial microPET and CT coregistered images obtained from mice at the indicated time following intratracheal administration of ^{76}Br-labeled particles described in Figure 1. (B) Three-dimensional reconstructions of PET scan activity (blue) merged with x-ray CT images that were signal-adjusted to reveal the skeleton (yellow). Arrows indicate gastrointestinal tract activity. Fiduciaries (f) used for co-registration are included. (C) The standardized uptake values (SUV) of the PET activity within the lung region from images as in (A), shown as the mean ± S.D. of 3–4 mice per particle type. 81×112mm (600 × 600 DPI)

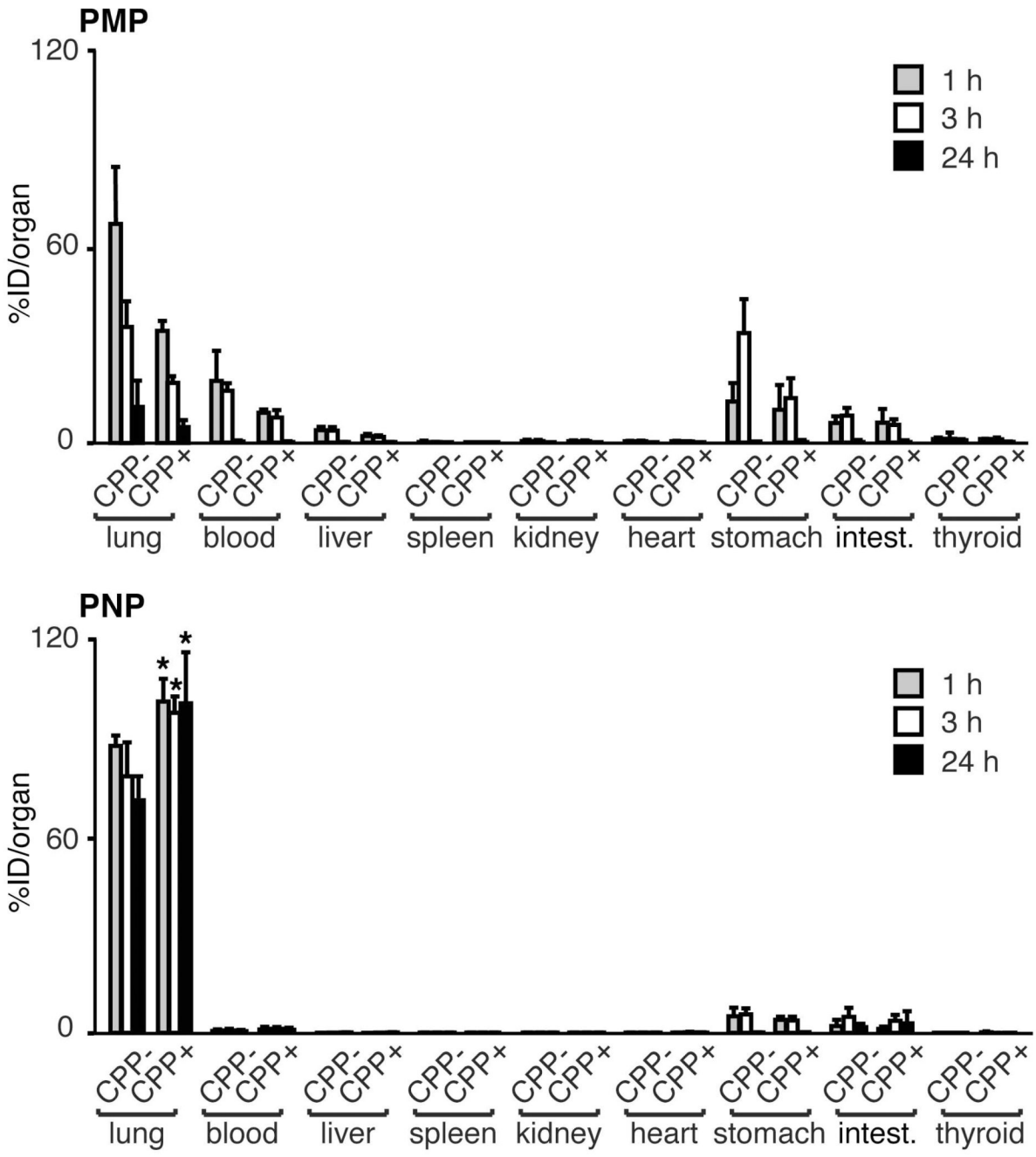

Figure 3.

Lung retention and biodistribution of particles following intratracheal delivery. Biodistribution of ^{125}I-labeled particle activity in the indicated organs performed 1, 3, and 24 h post-delivery. Activity was determined as the mean ± S.D. of the percent of the injected dose per organ (% ID/organ) from 3–5 mice per group. Particles were functionalized without (CPP−) or with (CPP +) Arg_9. The lung activity of PNP CPP+ was significantly greater than PNP CPP− at all times (*$p<0.05$). 81×97mm (600 × 600 DPI)

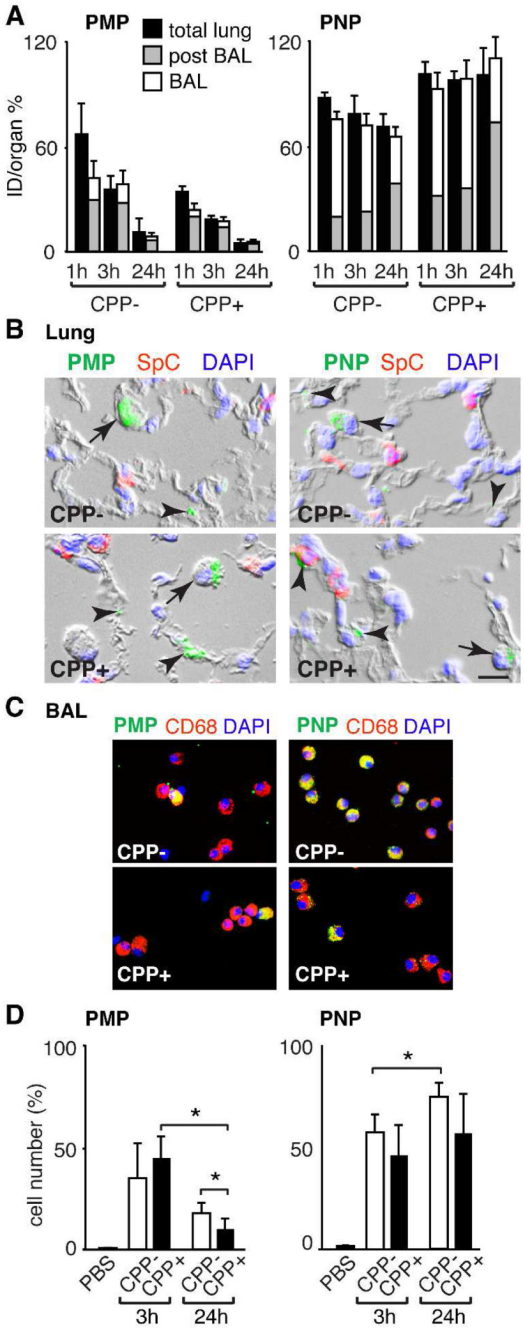

Figure 4.

Localization of particles in the lung following intratracheal delivery. (A) Activity of the indicated ^{125}I-labeled particle 1, 3 and 24 h post-delivery in the total lung, post-BAL lung and BAL fluid determined as the mean ± S.D. of the percent of the intratracheal dose per organ (% ID/organ) from 3–5 mice per group. (B) Photomicrographs of lung sections obtained 24 h after particle delivery show BSA-488-labeled particles (green) in alveolar epithelial cells (arrowheads) and cells with alveolar macrophage morphology (arrows). Tissue sections were stained to identify alveolar type II epithelial cells (prosurfactant protein C, SPC; red) and nuclei (DAPI; blue). Bar = 10 μm. (C) Photomicrographs of cells obtained by BAL 24 h after delivery of BSA-488-labeled particles that were immunostained with alveolar macrophage marker

antibody CD68 (red) and DAPI (blue). (D) Quantification of BAL alveolar macrophages that contain BSA-488-labeled particles. At 3 and 24 h post-delivery of PBS or particles, cells recovered in BAL fluid were immunostained for macrophage marker F4/80 and analyzed by flow cytometry. Shown is the mean ± S.D. of the percentage of macrophages containing BSA-488-labeled particles in 3–5 mice per group (*$p<0.05$). 63×168mm (600 × 600 DPI)

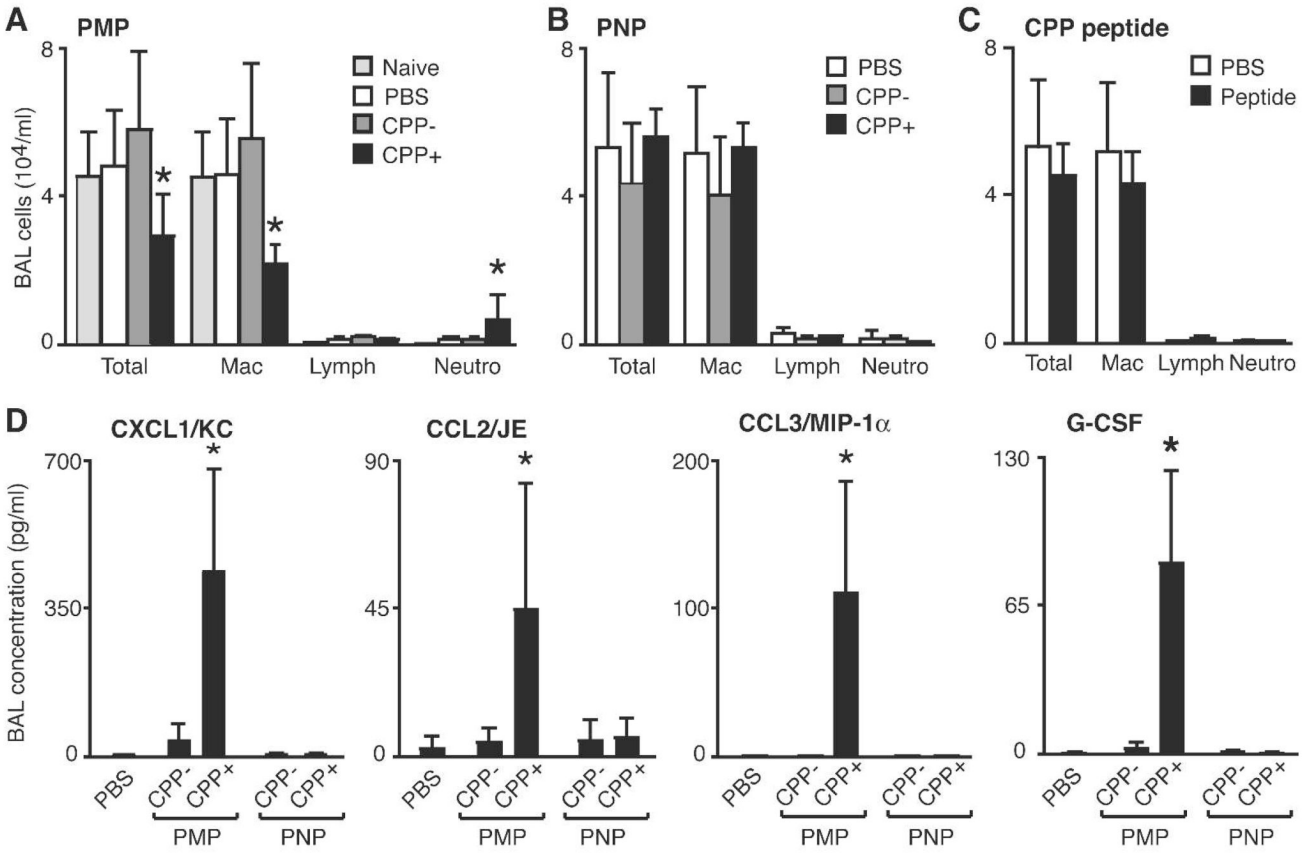

Figure 5.

Inflammatory response in the lung following intratracheal delivery of particles. (A-C) Quantification of cell types recovered by BAL 24 h post-delivery of the indicated particle or Arg_9 alone. Shown is the mean ± S.D. of total and individual cell types (Mac, alveolar macrophage; Lymph, lymphocyte; Neutro, neutrophil) from at least 3 mice. (D) BAL fluid cytokines measured in cell-free supernatant by BioPlex assay from 3 mice. A significant difference compared to other treatments is indicated (*$p<0.05$). 133×97mm (600 × 600 DPI)

Table 1

Properties of nanoparticles tested for respiratory tract delivery[a]

Particle Type	Hydrated Diameter[b]	Peptide (CPP)	Zeta-potential[b]	Cargo	Radiolabels
PMP CPP−	1.8 ± 1.2 μm	None	−0.1 ± 4.5 mV	BSA-488	^{125}I, ^{76}Br
PMP CPP+	2.7 ± 1.4 μm	Arg_9	+12.3 ± 4.0 mV	BSA-488	^{125}I, ^{76}Br
PNP CPP−	31.0 ± 9.3 nm	None	+7.6 ± 4.8 mV	BSA-488	^{125}I, ^{76}Br
PNP CPP+	31.7 ± 14.5 nm	Arg_9	+11.9 ± 4.0 mV	BSA-488	^{125}I, ^{76}Br

[a] Abbreviations: PMP, polyacrylamide microparticle; PNP, polyacrylamide nanoparticle; CPP, cell-penetrating peptide; Arg_9, nona-arginine peptide; BSA-488, bovine serum albumin-Alexa Fluor 488 conjugate.

[b] Mean ± S.D.

Table 2

Fate of nanoparticles following respiratory tract delivery[a,b]

Particle type	Lung retention	GI clearance	Blood transit	AM uptake	Epithelial uptake	Inflammation
PMP CPP−	++	++++	++	++	+	−
PMP CPP+	++	+++	++	++	+	+
PNP CPP−	++++	+	+	++++	+	−
PNP CPP+	++++	+	+	+++	+	−

[a] Abbreviations: GI, gastrointestinal; AM, alveolar macrophage.

[b] Scoring: −, not detected +, <10%; ++, 10–25%; +++, 26–50%; ++++, >50%